UNIVERSITÄT AUGSBURG
Universitätsbibliothek

OPEN ACCESS
OPUS AUGSBURG

The advent of fully variational quantum eigensolvers using a hybrid multiresolution approach

Fabian Langkabel, Stefan Knecht, Jakob S. Kottmann

Angaben zur Veröffentlichung / Publication details:

Langkabel, Fabian, Stefan Knecht, and Jakob S. Kottmann. 2026. "The advent of fully variational quantum eigensolvers using a hybrid multiresolution approach." *APL Computational Physics* 2 (2): 026106. https://doi.org/10.1063/5.0316008.

Nutzungsbedingungen / Terms of use:

CC BY 4.0

Dieses Dokument wird unter folgenden Bedingungen zur Verfügung gestellt: / This document is made available under these conditions:
CC-BY 4.0: Creative Commons: Namensnennung
Weitere Informationen finden Sie unter: / For more information see:
https://creativecommons.org/licenses/by/4.0/deed.de

APL Computational Physics

RESEARCH ARTICLE | MAY 14 2026

The advent of fully variational quantum eigensolvers using a hybrid multiresolution approach

Fabian Langkabel ; Stefan Knecht ; Jakob S. Kottmann

Check for updates

APL Computational Physics 2, 026106 (2026)
https://doi.org/10.1063/5.0316008

View Online Export Citation

Articles You May Be Interested In

Efficient ground state preparation in variational quantum eigensolver with symmetry-breaking layers

Minimizing energy consumption in hydrotechnical systems based on the integration of classical and quantum optimization approaches

AIP Conf. Proc. (August 2026)

Artificial-intelligence-driven shot reduction in quantum measurement

Chem. Phys. Rev. (October 2024)

16 October 2026 14:53:26

AIP Publishing

APL Computational Physics ARTICLE pubs.aip.org/aip/aco

The advent of fully variational quantum eigensolvers using a hybrid multiresolution approach

Cite as: APL Comput. Phys. 2, 026106 (2026); doi: 10.1063/5.0316008
Submitted: 10 December 2025 • Accepted: 30 March 2026 •
Published Online: 14 May 2026

View Online Export Citation CrossMark

Fabian Langkabel,[1,a] Stefan Knecht,[1] and Jakob S. Kottmann[2,3,b]

AFFILIATIONS

[1] Algorithmiq Ltd., Kanavakatu 3C, FI-00160 Helsinki, Finland
[2] Institute for Computer Science, University of Augsburg, Augsburg, Germany
[3] Center for Advanced Analytics and Predictive Sciences, University of Augsburg, Augsburg, Germany

[a] **E-mail:** fabian.langkabel@algorithmiq.fi
[b] **Author to whom correspondence should be addressed:** jakob.kottmann@uni-a.de

ABSTRACT

In electronic structure theory, variational computing offers a valuable paradigm for the approximation of electronic ground states. However, for historical reasons, this principle is mostly restricted to model chemistries in predefined fixed basis sets. Especially in quantum computation, these model chemistries are far from an accurate description of the initial electronic Hamiltonian. This work demonstrates a *fully* variational approach to the electronic structure problem by variationally optimizing the orbitals representing the second quantized Hamiltonian alongside a quantum circuit that generates the many-electron wavefunction. To this end, the orbitals are represented within an adaptive multi-wavelet format, guaranteeing numerical precision. We then showcase explicit numerical protocols and highlight the quantum circuit's effects on determining the optimal orbital basis.

© 2026 Author(s). All article content, except where otherwise noted, is licensed under a Creative Commons Attribution (CC BY) license (https://creativecommons.org/licenses/by/4.0/). https://doi.org/10.1063/5.0316008

16 October 2026 14:53:26

I. INTRODUCTION

In the long term, the hope for quantum computers is to increase the applicability of (near-exact) quantum chemical calculations. A central algorithm here is quantum phase estimation[1] that can compute accurate eigenenergies of a given second-quantized Hamiltonian. The only remaining source of error with respect to the original electronic Schrödinger equation is the finite orbital basis, used to construct the second quantized Hamiltonian from the original real-space operator. Execution of such energy estimations is currently anticipated to be computationally expensive,[2–4] which motivated the development of optimal representations with respect to the chosen orbital basis. The standard approach is to select an active space of orbitals where the quantum computation takes place, followed by repeatedly rotating this active space within the fixed space of the basis orbitals. In order to operate in the optimal orbital basis on a given number of available qubits, essentially two conditions need to be satisfied: (1) the underlying atom-centered Gaussian basis set needs to be sufficient to represent the optimal orbitals, and (2) the orbital-optimization algorithm needs to converge. By choosing a large (correlation-consistent) basis set (e.g., d-aug-cc-pCV6Z), the first condition can, in principle, always be satisfied such that no domain expertise is necessary to ensure a sufficient quality of the basis set. The resulting calculations are, however, far from feasible—this is due to the increased computational cost of the underlying orbital optimization as well as decreased empirical heuristics to initialize the parameters of the orbital optimization in such large basis sets. The second condition is also challenging, as the selection of active spaces alone is already not trivial[5,6] and an ongoing research topic.[7–12]

A prominent alternative to phase estimation is variational algorithms that deal with the expectation values of electronic Hamiltonians. In the long term, they are expected to provide useful initial states to increase the success probabilities of direct energy measurement. Although computationally more tractable, the evaluation of these expectation values and the optimization of the underlying quantum

© Author(s) 2026

circuits are still considered costly, so that optimal bases are again desirable.

In this work, we will investigate the direct construction of second-quantized electronic Hamiltonians by representing the spatial orbitals in a formally complete basis of multiwavelets. Starting from an initial guess of spatial functions, the active orbitals are further refined by solving an integral equation defined by the current solution of a variational quantum algorithm. We will start with the technical background in electronic structure and multiwavelet representations, followed by a brief summary of variational quantum eigensolvers. In Sec. III, we will provide details of the main algorithms and their implementations and assess their numerical performance by means of molecular examples in Sec. IV.

II. TECHNICAL BACKGROUND

This work builds up from a series of prior studies that all focus on the determination of numerically exact real-space representations of chemical systems in a black-box fashion. Further below, the broader background is illuminated, while we summarize the developments most important for this work in this paragraph. In Ref. 13, Kottmann, Bischoff, and Valeev realized the first attempt to determine optimal orbitals in an adaptive real-space basis from scratch, essentially reaching the basis set limit with affordable runtime. Here, the correlated many-body method was Møller–Plesset Perturbation Theory (MP2), and the determined orbitals were pair-natural orbitals (PNOs). As a follow-up, Kottmann and Aspuru-Guzik *et al.* employed the optimal PNOs to construct second-quantized Hamiltonians that can then be tackled with the full toolset of classical quantum chemistry [e.g., coupled-cluster or configuration interaction (CI)] as well as variational quantum algorithms, realizing the first hybrid approach that couples adaptive real-space orbital determination with general many-body methods.[14] Here, the notion of a surrogate functional to determine the optimal orbital basis was introduced—in this methodology, the basis error is solely determined by the quality of the surrogate functional. In a further study, the same authors adapted the variational quantum circuits (many-body part) to the surrogate model (one-body-part), leading to the separable pair-approximation.[15] In Ref. 16, Valeev *et al.* derived the equations to determine optimal orbitals for general many-body methods. In the terminology of previous studies, these equations determine an exact surrogate potential depending on the reduced density matrices of an arbitrary many-body method.

This work functions as a bridge between the surrogate functional of Ref. 14 and Valeev's functional,[16] where we focus on the application domain of quantum computation and the interdependence of the quality of the determined orbital-bases with the used quantum circuits.

After the initial release of this work, Nibbi *et al.* released a preprint[17] investigating the combination of Valeev's functional with the Density Matrix Renormalization Group (DMRG) for the many-body part.

We note that different approaches formulated in real space,[18–20] as well as methods to directly optimize Gaussian-based basis sets (e.g., pioneering studies by Tamayo-Mendoza *et al.*[21] using automatic differentiation; see also Refs. 22 and 23 and recent studies[24]) have also been investigated.

In the following, we will give an overview of the individual fields of research essential to this work.

A. The electronic structure problem

The electronic structure problem of quantum chemistry aims to approximate the eigenstates of electronic Hamiltonians,

$$H = \sum_{k=1}^{N_e} h(r_k) + \frac{1}{2}\sum_{k\neq l}^{N_e} g(|r_k - r_l|), \tag{1}$$

with $r_k \in \mathbb{R}^3$ being a spatial coordinate of an electron and $h(r_k)$ being the corresponding one-body energy operator $h(r_k) = T(r_k) + V(r_k)$ consisting of the kinetic energy operator T and an external potential V—typically a Coulomb potential of point charges generated by nuclei in a given molecule—in which the electrons move. The two-body operator $g(r_k - r_l) = 1/(\|r_k - r_l\|)$ is the electrostatic repulsion between two electrons at points r_k and r_l. In the absence of magnetic fields, the Hamiltonian is independent of the electron spin, which is usually introduced *ad hoc* to the electronic wavefunction. The state of an isolated electron can be described as a function $\psi(r,s) = \phi(r) \otimes |s\rangle$, with spatial part $\varphi \in L^2(\mathbb{R}^3)$ (note that the choice of L^2 is somewhat pragmatic here, and the Hilbert space of ϕ can be restricted further as a proper subspace of L^2—see, for example, Ref. 25, Chapter 2.3) and spin state $|s\rangle \in \mathrm{span}\{|\uparrow\rangle, |\downarrow\rangle\}$. Building up from the one-electron spaces, we can construct spaces for many-electron wavefunctions as anti-symmetric tensor products. A more convenient and dominantly used form of the electronic Hamiltonian is in its second quantized form using the anti-commuting field operators[26] $\hat{\psi}(r,s)$ ($\hat{\psi}^\dagger(r,s)$) that annihilate (create) electrons with spin s at the spatial coordinate r,

$$H = \sum_{s\in\{\uparrow,\downarrow\}} \int \mathrm{d}r\, \hat{\psi}^\dagger(r,s) h(r) \hat{\psi}(r,s) + \frac{1}{2}\sum_{s_1,s_2\in\{\uparrow,\downarrow\}} \int \mathrm{d}r_1 \int \mathrm{d}r_2\, \hat{\psi}_1^\dagger \hat{\psi}_2^\dagger g_{12} \hat{\psi}_1 \hat{\psi}_2, \tag{2}$$

where we used $\hat{\psi}_n \equiv \hat{\psi}(r_n, s_n)$ and $g_{12} = g(|r_1 - r_2|)$ for brevity. The operator can be interpreted as probing each spatial point and assigning the corresponding energies if electrons are present. The second quantized form given above in Eq. (2) is admittedly not ideal for numerical methodologies, such that a more prominent version exploits a discretized form where the field operators are expanded into a set of different operators a_k ($a_k^\dagger$) that annihilate (create) electrons with spin s_k in the spatial orbital ϕ_k,

$$\hat{\psi}(r,s) = \sum_k \phi_k(r)|s\rangle a_k, \tag{3}$$

$$\hat{\psi}^\dagger(r,s) = \sum_k \langle s|\phi^*(r) a_k^\dagger. \tag{4}$$

The formal assumption in the above expansions is that the spatial functions $\{\phi_k(r)\}$ are dense in the three-dimensional Hilbert space $\mathbb{L}^2$. Inserting the expansions (3) and (4), respectively, in Eq. (2) leads to the usual form of the second-quantized Hamiltonian

$$H = \sum_{kl} h_{kl} a_k^\dagger a_k + \frac{1}{2}\sum_{klmn} g_{mn}^{kl} a_k^\dagger a_l^\dagger a_n a_m, \tag{5}$$

16 October 2026 14:53:26

© Author(s) 2026

with the tensors $h_{kl} = \langle\phi_k|h|\phi_l\rangle\langle s_l|s_k\rangle$ and $g^{kl}_{mn} = \langle\phi_k\phi_l|g_{12}|\phi_m\phi_n\rangle\langle s_k|s_m\rangle\langle s_l|s_n\rangle$ defined via integrals of the corresponding orbitals and spins with the one- and two-body operators. Note that a set of suitable basis functions ϕ_k has to be introduced here, which simplifies the original electronic structure problem so that the Hamiltonians from Eqs. (1) and (5) are not equivalent anymore. The central assumption is that the chosen set of basis functions represents the chemically relevant wavefunctions well enough that these differences become negligible. The most common approach in quantum chemical applications is the use of fixed sets of atom-centered basis functions (basis sets).

B. Multiresolution analysis

In the context of this work, we leverage multiwavelets to numerically represent the basis orbitals that define the second-quantized operator in Eq. (5). In the following, the basics of multiresolution analysis (MRA) are captured briefly. The main advantages are that, in contrast to atom-centered orbitals, MRA constructs a complete orthonormal basis of $L^2(D)$ (the Hilbert space of quadratically integrable functions on the domain D) on a finite simulation domain $D = [-L, L]^d$ with dimension d that can be truncated in a systematic and individual manner. To illustrate the basics, we will use $d = 1$ and $L = 1$. A complete orthonormal basis of $L^2(D)$ is given by the Legendre polynomials $\{P_n(x)\}_{n\in\mathbb{N}}$. If we truncate this set by restricting the maximal order n to a finite integer k, we receive an approximation of $L^2(D)$ spanned by these polynomials $V_0 = \mathrm{span}\big(\{P_m(x)\}_{m<k}\big)$. By increasing k, we can increase accuracy, but we will not have much control over it. Alternatively, we can keep the initial k fixed and divide the domain $D = [-1, 1]$ in the middle. This leads to two new non-overlapping domains $D^0_1 = [-1, 0]$ and $D^1_1 = [0, 1]$, on which we can define two new sets of polynomials up to order k that span the vector spaces V^0_1 and V^1_1 (outside of the corresponding domain, the polynomials will be set to zero). Each of the new sets of polynomials will be derived from the original set by shifting and rescaling, $V^0_1 = \mathrm{span}\Big(\Big\{\frac{1}{2}P_m(2x-1)|_{x\in D^0_1}\Big\}_{m<k}\Big)$, and correspondingly for V^1_1. Our total approximation space is then given by the direct sum of the two spaces representing the left and right parts of the original domain D (note that through the piecewise definition, the corresponding functions remain orthogonal). We can repeat this process recursively in order to locally increase the resolution of the domain D. The general approximation space is given by $V^l_n = \mathrm{span}\Big\{2^{n/2}P_k(2^n x - l)\Big\}$, which will resolve the subdomain $D^l_n = [l\cdot 2^n, (l+1)\cdot 2^n]$ with the rescaled and shifted k polynomials. Here, n denotes the refinement level that also restricted the spatial interval through $l \in [0, 2^n - 1]$. Key to an automatized truncation of the local resolution is the wavelet spaces W^l_n that span the orthogonal complement between two levels: $V^l_n \oplus W^l_n = V^{2l}_{n+1} \oplus V^{2l+1}_{n+1}$. It suffices to compute the wavelets that span $W_0 \equiv W^0_0$ and apply the same shifting and rescaling procedure as for the polynomials before to obtain the wavelets of W^l_n. An arbitrary function f can now be represented by the original k polynomials (the space V_0) supplemented with an arbitrary deep refinement of the wavelet spaces W^l_n. A complete representation that is dense in $L^2(D)$ is

$$L^2(D) = \overline{V_0 \bigoplus_{n\in\mathbb{N}_0}\Big(\bigoplus_{0\le l\le 2^n-1} W^l_n\Big)}. \tag{6}$$

Since each wavelet space has two children, we can represent this construction as a binary tree. A function f can now be represented with arbitrary accuracy by starting at the root (or a full-tree arbitrary level n to avoid undersampling) and recursive refinement. Once the norm of wavelet coefficients of a specific level W^l_n falls below a given accuracy threshold, the refinement can be stopped.

Higher dimensional representations can be constructed via specific tensor products between the low-dimensional spaces. A two-dimensional MRA can, for example, be constructed as $V^{(d=2)}_0 = V^{d=1}_0 \otimes V^{d=1}_0 = \{P_{m_1}(x)P_{m_2}(y)\}_{m_1,m_2<k}$. The shifting and rescaling procedure stays the same, just that we now have four children of each parent space, splitting the two-dimensional domain into four quadrants. Correspondingly, there are also four wavelet spaces, constructed from the direct tensor product of W_0 and the three possible combinations of V_0 and W_0. Operators follow essentially the same construction pattern, and the details are omitted here.

An MRA is a proper basis of L^2 and is, therefore, in the context of quantum chemistry, often referred to as a *basis-set-free* representation. Software packages such as MADNESS[27] or MRCHEM[28,29] implement high-level access to MRA technology in an intuitive way that is sometimes referred to as a *basis-free* formulation, as the user can choose to ignore the details of the underlying numerical representation entirely. Consider, for example, two analytically known functions and their product,

$$f(x) = e^{-|x|}, \quad g(x) = x^2, \quad p(x) = g(x)\cdot f(x). \tag{7}$$

A *basis-free* implementation would take the following form:

```
1 def functor_f(x) = exp(-abs(x))
2 def functor_g(x) = x**2
3 f = project(functor_f)
4 g = project(functor_g)
5 p = f*g
```

The so-constructed MRA representation of f, g, p is carried out fully automatized in the background and, in practice, guarantees an accurate representation up to a given threshold.

C. Multiresolution quantum chemistry

In the following, we will highlight the general strategy of directly determining quantum states for quantum chemistry, followed by a brief overview of existing work. Schrödinger's equation for a single electron in a potential V is

$$\Big(-\frac{\Delta}{2} + V(r)\Big)\Psi(r) = E\Psi(r). \tag{8}$$

We can rearrange this equation to obtain a defining equation for the quantum state,

16 October 2026 14:53:26

© Author(s) 2026

$$\Psi(r) = -2(-\Delta - 2E)^{-1} V(r)\Psi(r), \tag{9}$$

where the inverse of the shifted Laplacian [or a bound-state Helmholtz (BSH) operator] is an integral operator with the Helmholtz Green's function in three dimensions,

$$(-\Delta + \mu^2)G_\mu(r) = \delta(r), \quad G_\mu = \frac{e^{-i\mu r}}{4\pi r} \tag{10}$$

as kernel. Altogether, Eq. (9) can be written as

$$\Psi(r) = -2\int G_\mu(r - r')V(r')\Psi(r')\mathrm{d}r', \tag{11}$$

with $\mu = \sqrt{-2E}$. The quantum state $\Psi(r)$ can be determined by a fixed-point approach starting with an initial guess for $\Psi(r)$ and repeatedly inserting into the above equation with updated μ via expectation values. Most methods in quantum chemistry lead to similar equations—the main difference being that the potential $V(r)$ is usually not a multiplicative potential of an analytically given function anymore. We can summarize the procedure for most quantum chemical methods as follows:

1. Choose an initial guess of orbitals $\{\phi_i\}$ and represent each of them through an MRA tree.
2. Construct the defining equations for each orbital in the following form:

$$\phi_k(r) = \int G_\mu(r - r')V_k[\{\phi_i\}](r')\mathrm{d}r', \tag{12}$$

   where the potential V_k usually depends on all orbitals, and the definition of μ depends on the method.
3. Solve Eq. (12) by iteratively computing the potentials V_k, updating the orbitals according to the defining equation, and orthonormalizing the updated orbitals.

For example, in the case of restricted Hartree–Fock for a system with N_e electrons in an external potential $V(r)$, the Schrödinger-like equation is

$$\left(-\frac{\Delta}{2} + V(r) + 2J - K\right)\phi_k(r) = \epsilon_k\phi_k(r), \tag{13}$$

which has to be solved for a set of orthonormal orbitals $\{\phi_k\}_{k=1}^{N_e/2}$ and orbital energies $\{\epsilon_k\}_{k=1}^{N_e/2}$. After a similar rearrangement, we end up with defining equations for the orbitals

$$\phi_k = -2\int G_\mu(r - r')V_{HF_i}(r')\mathrm{d}r', \tag{14}$$

with $\mu = \sqrt{-2\epsilon_k}$, and the potential[30–32]

$$V_{\mathrm{HF}_i}(r) = (V(r) + 2J - K)\phi_i(r) = V(r)\phi(i) + 2\left(\sum_k g_k^k(r)\right)\phi_i(r) - \sum_k g_i^k(r)\phi_k(r) \tag{15}$$

with the abbreviation

$$g_k^l(r) = \left(\int g_{12}(r - r')\phi_k(r')\phi_l(r')\mathrm{d}r'\right). \tag{16}$$

In passing, we note that in quantum chemistry, HF is usually only the first step of more complex calculations due to a poor description of the electron correlation. In order to describe the missing correlation, these methods include additional, initially unoccupied orbitals, the so-called virtual orbitals, in the many-body wavefunction. While these virtual orbitals are obtained as a by-product of the Roothaan–Hall procedure (HF in a fixed basis), this is not the case with MRA representations that typically tackle the HF equations directly by iteratively solving the fixed-point equation (33). The challenge for post-HF methodology is to generate a set of virtual orbitals that can describe the missing correlation as accurately as possible with as few orbitals as possible. In the early days of MRA quantum chemistry, this was often circumvented by solving the corresponding methods, such as MP2[33,34] and CC2,[35–37] directly by representing the occurring electron-pair functions with six-dimensional MRA trees. The first demonstration of a post-HF with adaptively refined one-body functions was a many-body perturbation method (PNO-MP2-F12).[13] For this purpose, pair-natural orbitals (PNOs) were generated as virtual orbitals, which represent the optimal solution to the problem (PNOs used in this work will always refer to the PNOs of Ref. 15 obtained without explicit correlation and using the "diagonal" approximation).

More recently, going beyond single-reference *Ansätze*, Valeev and co-workers developed a procedure for describing arbitrary MRA-based many-body wavefunctions together with a protocol to determine optimal virtual orbitals.[16] In the latter work, they used full CI and Heat-Bath CI (HCI) as exemplary post-HF methods and started with virtual orbitals based on finite (Gaussian-type) basis sets. Apart from multiwavelets, approaches based on Daubechies wavelets[19] and optimized Gaussian basis sets via gradient-based approaches[21,22,38] have been investigated as alternatives to fixed Gaussian basis sets and have been demonstrated on mean-field HF. For example, in Ref. 38, the orbitals from a Gaussian basis set were contracted through intrinsic contraction. Moreover, in contrast to this work, where multiwavelets in a discontinuous Galerkin fashion are used to represent orbitals that form the second quantized Hamiltonian, Ref. 39 investigated a direct construction in the numerical basis.

Apart from traditional "wavefunction" based methodologies, the MRA representation has been applied to density functional theory,[31,40–42] orbital effective potentials,[43] range-separation,[44,45] magnetic and optical properties,[46–48] solvation models,[49,50] and even relativistic approaches.[51–55] Although seemingly unrelated at first glance, these developments and their open-source implementations within the two main packages MADNESS[27,56] and MRCHEM/VAMPYR[28,29] are crucial to this work as well as open up for possible future extensions of our present approach beyond pure ground-state energy estimations.

To summarize, our algorithm, detailed in Sec. III, exploits ideas from previous studies in multiresolution quantum chemistry. Starting from HF MRA orbitals,[30,57] PNOs[13] are generated and optimized via Eq. (33) to serve as initial functions for the methodology in Sec. III. Subsequently, the h_{kl} and g_{mn}^{kl} tensors are obtained directly by integration on the MRA representation, and the resulting Hamiltonian is used to calculate many-body wavefunctions and reduced density matrices (RDMs) via a second-quantized variational procedure.[14] To optimize many-body wavefunctions, we employ (i)

16 October 2026 14:53:26

© Author(s) 2026

a variational quantum eigensolver (see Sec. II D) and (ii) a standard full CI solver. The calculated RDMs η^l_k and η^{mn}_{kl} are then used to refine the MRA orbitals similar to Ref. 16 but using our own implementation.

D. Variational quantum eigensolvers

The basic idea of variational quantum computing can be summarized into a three-step procedure: (1) represent the electronic Hamiltonian [Eq. (5)] of N spin orbitals as an operator, commonly referred to as qubit Hamiltonian, on N qubits; (2) construct a parameterized quantum circuit, execute it on a quantum processor, and measure the expectation value of the qubit Hamiltonian; and (3) update the parameters of the circuit to lower the energy expectation value and repeat until convergence. Fortunately, the gradients of expectation values can be measured as well[58,59] so that standard classical optimization procedures can be employed. After the optimal parameters of the circuit are determined, it can be used to prepare the electronic ground state approximation Ψ, and general observables can be measured. In this work, the observables of interest are the RDMs that can be written as expectation values with respect to the quantum state Ψ,

$$\gamma^l_k = \langle a^\dagger_l a_k \rangle_\Psi, \quad \gamma^{mn}_{kl} = \langle a^\dagger_m a^\dagger_n a_k a_l \rangle_\Psi, \tag{17}$$

where we will explicitly require spin-summed reduced density matrices that only depend on the indices of the spatial orbitals,

$$\eta^l_k = \sum_{\sigma \in \{\uparrow,\downarrow\}} \gamma^{l\sigma}_{k\sigma}, \quad \eta^{mn}_{kl} = \sum_{\sigma,\tau \in \{\uparrow,\downarrow\}} \gamma^{m\sigma n\tau}_{k\sigma l\tau}. \tag{18}$$

The first step (encoding the second-quantized Hamiltonian) is to represent it in the standard Pauli form,

$$H = \sum_k c_k P_k, \tag{19}$$

where P_k are Pauli-strings (tensor products of the Pauli matrices X, Y, Z). The most common encoding is Jordan–Wigner, where the second quantized operators are encoded quite naturally into the qubit raising and lowering operators $\sigma^\pm = \frac{1}{2}(X \pm iY)$ and a string of Z operators to ensure anti-commutativity,

$$a^\dagger_k = \left(\prod_{l<k} Z_l\right)\sigma^-_k, \quad a_k = \left(\prod_{l<k} Z_l\right)\sigma^+_k. \tag{20}$$

In the same way, we can then express the RDMs of Eq. (17) in the standard Pauli form.

The design of the quantum circuit is currently an active problem in research, and several methods have been proposed—see Refs. 60 and 61 for recent reviews. A significant fraction takes inspiration from unitary coupled-cluster (UCC), which provides unitary building blocks in the form of n-electron excitations. We can construct them with a list of tuples $[(k_0, l_0), (k_1, l_1), \ldots]$ that encode electronic exchanges between spin-orbitals (k_j, l_j) and result in the generator

$$G_n = i\left(\prod_j \left(a^\dagger_{k_j} a_{l_j}\right) - h.c.\right) \tag{21}$$

that itself generates the parameterized unitary

$$U(\theta) = e^{-i\frac{\theta}{2}G}. \tag{22}$$

The anti-Hermitian as $i(x - x^\dagger)$ ensures that the resulting unitary only creates real superpositions. The generators G_n can be decomposed into the standard Pauli form in the same way as it was done for the electronic Hamiltonian—in this case, the decomposition will result in a set of commuting Pauli strings[62] so that the compilation of a quantum circuit is straightforward (see, for example, Ref. 60 or 63 for a direct approach).

Pioneering studies proposed adaptations of the conventional Unitary Coupled-Cluster with Singles and Doubles (UCCSD)[62,64–66] method into the individual building blocks in Eq. (22) via Trotter decompositions. Over the following years, "bottom-up" strategies that assemble the UCC building blocks directly, e.g., through adaptive[67,68] or heuristic[69–73] strategies, have been demonstrated to be more effective in the cost-to-benefit ratio.

E. The separable pair approximation

In this work, we will employ mostly the separable pair approximation (SPA)[15] and some extensions of it, as the range of applicability of the approximation is understood, and the method has been shown to produce consistent results in several applications.[74–77] This allows us to create wavefunctions with controlled quality in their approximations and study the effects on the basis refinement. In the following, we will summarize the main idea and sketch the construction of the quantum circuits. For more details, see the original publication[15] as well as Refs. 78 and 79.

Although not strictly necessary, SPA circuits are usually restricted to the seniority zero sector of the many-body space, meaning that all electrons form spin-pairs and can be treated as quasiparticles, so-called hard-core Bosons (HCB). For N_o spatial orbitals, the corresponding quantum states can then be represented on N_o qubits. If desired, these states can be transformed to the spin-orbital representation with N_o controlled-not gates. The central idea of the separable pair approximation is, however, to approximate the N_e-electron quantum state as a product,

$$|\Psi\rangle = \bigotimes_{k=1}^{N_e/2} |\psi_k\rangle, \tag{23}$$

of $N_e/2$ electron-pair functions $|\phi_k\rangle$, defined on n_k qubits with the restriction $\sum_k n_k = N_o$, and no qubit can be shared between two pair functions. An individual electron-pair state can be initialized with a simple circuit consisting of (controlled-) not operations and $R_y(\theta) = e^{-i\frac{\theta}{2}Y}$ rotations,

$$U_k(\boldsymbol{\theta}^k) = \texttt{NOT}(0)\prod_{i=1}^{n_k} \texttt{CNOT}(i, i-1)\texttt{CRy}(i-1, i, \theta^k_i). \tag{24}$$

An example for such a circuit on six qubits is

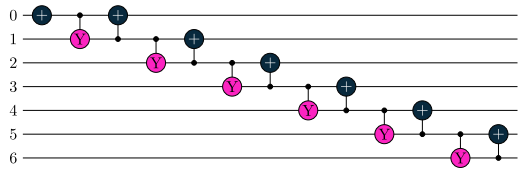

(25)

16 October 2026 14:53:26

© Author(s) 2026

where the control on the first Ry rotation can be removed for efficiency. Due to this construction, the final SPA circuits are comparably low in depth: Assuming a constant orbital per pair assignment, the depth is constant with system size and increases linearly with the number of orbitals per pair (see Table 1 of Ref. 15 for explicit examples).

SPA circuits are typically coupled with an orbital optimization, or alternatively, a sequence of generalized single-electron excitations after the initial circuit (indicated as SPA+GS). Both variants have the same expressibility, and the respective results only differ through the involved optimization algorithms. To apply the SPA in practice, the user needs to assign all orbitals to an electron pair. In the original work, this assignment was based on pair-natural orbitals (PNOs) and was later extended to a valence-bond picture where a resonance structure guides the assignment of orbitals as well as the initial guess in the orbital optimization. In this work, we stick to the PNO-based assignment. Note, however, that in the chosen test systems, this does usually correspond to the valence bond-based assignment.

F. MRA-PNOs

Here, we give a brief overview of how MRA-PNOs are generated. By default, this is performed in combination with Boys localization[80] and follows the computational protocols described in Refs. 13–15. As an initial step, the (occupied) Hartree–Fock orbitals $\{\phi_k^{HF}\}_{k=1}^{N_e/2}$ are generated.[30] For each HF orbital ϕ_k^{HF}, we compute a set of *diagonal* (see Ref. 15) PNOs $\{\phi_a^k\}_{a=1}^{n_k}$. As the individual PNO sets are not orthogonal by definition, they are symmetrically orthonormalized. The total set

$$\bigcup_{k=1}^{N_2/2} M_k = \bigcup_{k=1}^{N_2/2} \left(\{\phi_k\} \cup \{\phi_a^k\}_{a=1}^{n_k} \right) \tag{26}$$

consisting of $n_1 + n_2 + \cdots n_{N_e/2}$ spatial orbitals is then used as the one-body basis to construct the Hamiltonian in Eq. (5). In order to achieve a balanced description, we usually set the individual PNO ranks n_k to the same number. When combined with the SPA circuit (see Sec. II E), all orbitals in the sets M_k are assigned to an individual pair. Using `tequila` in combination with `madness`, Hamiltonian and circuits can be constructed and used as an input to a Variational Quantum Eigensolver (VQE) minimization in the following way:

```
1 mol = tequila.Molecule("coord.xyz")
2 H = mol.make_hamiltonian()
3 U = mol.make_ansatz(name="SPA")
4 E = tequila.ExpectationValue(H=H, U=U)
5 result = tequila.minimize(E)
```

Note that the PNO assignment to the SPA pairs happens automatically, while the default number of orbitals corresponds to two spatial orbitals per active electron pair—the equivalent of a minimal basis. We refer to the Appendix of Ref. 15 and the evolving codebase for more options.

III. FULLY VARIATIONAL QUANTUM CHEMISTRY

The overall goal of the electronic structure ground state problem given in Eq. (2) can be rephrased to *fully* minimize the many-body energy,

$$E[\Psi, \{\phi_k\}] = \sum_{kl} \eta_k^l h_k^l + \frac{1}{2} \sum_{klmn} \eta_{kl}^{mn} g_{kl}^{mn}, \tag{27}$$

here given as a functional of a second-quantized many-body wavefunction Ψ and a spatial orbital basis $\{\phi_k\}$. The one- and two-body RDMs η_k^l and η_{kl}^{mn} [cf. Eq. (17)], respectively, are obtained from Ψ, while the one- and two-body coefficients h_k^l, g_{kl}^{mn} are dependent on $\{\phi_k\}$ as can be seen in Eq. (4). By invoking the variational principle

$$E_0 \leq \min_{\Psi, \{\phi_k\}} E, \tag{28}$$

the latter will yield the true ground state energy E_0 with respect to the original first-quantized Hamiltonian given in Eq. (1). To achieve this goal, we set out from a sequential minimization of a parameterized many-body wavefunction $\Psi(\boldsymbol{\theta})$ for a fixed set of orbitals in the form of a VQE run, followed by a variation of the orbital basis for a fixed set of RDMs. The resulting procedure is then repeated until convergence. Whereas the first step is outlined already in Sec. II D, the orbital variation step deserves further discussion.

While the many-body wavefunction is parameterized in a discretized form through parameterized quantum gates, the variation of the orbitals is performed in a continuous fashion. The Lagrangian

$$\mathcal{L} = E[\Psi, \{\phi_k\}] - \sum_{kl} \epsilon_{kl} (\langle \phi_k | \phi_l \rangle - \delta_{kl}) \tag{29}$$

results directly from the energy functional in Eq. (28) but also takes the orthonormalization of the spatial orbital basis $\{\phi_k\}$ explicitly into account through the last term. Stationary conditions can now be obtained by requiring the functional derivative to vanish,

$$\frac{\delta}{\delta \phi_i} \mathcal{L} = 0. \tag{30}$$

Taking the functional derivative of the first term in the Lagrangian will reveal the Laplacian hidden in the one-body integrals,

$$\begin{aligned} \frac{\delta}{\delta \phi_i} \sum_{kl} h_k^l \eta_l^k &= \sum_{kl} \frac{\delta}{\delta \phi_i(r)} \int \phi_l(r') h(r') \phi_k(r') \mathrm{d}r' \eta_l^k \\ &= \sum_{kl} 2h(r) \phi_k(r) \delta_{il} \eta_l^k \\ &= 2 \sum_k \left(-\frac{1}{2} \nabla^2 \phi_k(r) + V(r) \phi_k(r) \right) \eta_i^k. \end{aligned} \tag{31}$$

The stationary condition for the whole Lagrangian is then given by the differential equation

$$2 \sum_k \left(-\frac{1}{2} \nabla^2 \phi_k(r) + V(r) \phi_k(r) \right) \eta_i^k + \frac{\delta}{\delta \phi_i} \mathcal{V} = 0, \tag{32}$$

where $\mathcal{V}$ comprises the second and third terms in the energy functional of Eq. (27) given above. Following Valeev and co-workers,[16] we can transform the orbitals into natural orbitals by diagonalizing

16 October 2026 14:53:26

© Author(s) 2026

the reduced one-body density matrix η_i^k, which will eliminate all Laplacian terms with $k \neq i$ in the sum above. This results in the defining equations for the stationary orbitals,

$$\phi_i = -2\hat{G}_{-\frac{\epsilon_i^i}{\eta_i^i}}\left(\hat{V}\phi_i - \frac{1}{\eta_i^i}\sum_{k\neq i}\epsilon_k^i\phi_k + \frac{1}{\eta_i^i}\sum_{lnk} g_l^n \eta_{kl}^{in}\phi_k\right), \tag{33}$$

where $\hat{G}_\mu = \left(\nabla^2 - \mu\right)^{-1}$ is the bound-state Helmholtz Green's operator, and the Lagrange multipliers ϵ_a^i are given as

$$\epsilon_a^i = \eta_i^i h_a^i + \sum_{lnk} \eta_{kl}^{in} g_{al}^{kn}. \tag{34}$$

In a general form, Eq. (33) can be written as

$$\phi_i = -2\hat{G}_{\mu_i}\mathcal{V}_i[\{\phi_k\}] \tag{35}$$

with a potential operator $\mathcal{V}_i[\{\phi_k\}]$ for each orbital ϕ_i that is also functional of all orbitals. Using the terminology of Ref. 14, this is the surrogate potential that determines the basis of the electronic system. Valeev's potential (33) denotes an exact potential, while the PNO-based potential of Ref. 13 is an approximation. In the same way, a mean-field potential could be used, but this typically results in unbounded virtual orbitals, i.e., for most molecular systems, we would only obtain $N_e/2$ bound solutions.

Since the orbital update of each orbital also depends on all other orbitals, the update is performed iteratively until all orbitals converge. For faster convergence, more efficient solvers can be used instead of the fixed point update shown in Eq. (33)—historically, the KAIN[81] approximation has proven useful here. Since the update of all orbitals is performed simultaneously without updating the integrals within an iteration step, the orthonormality of the orbitals is no longer given after an iteration step, which makes reorthonormalization after each iteration step necessary. To this end, we make use of the symmetric ("Löwdin") orthogonalization following Ref. 15. After the convergence of all orbitals, the new h_{kl} and g_{mn}^{kl} tensors are used to update the Hamiltonian of the quantum part for optimization of the many-body wavefunction $\Psi(\boldsymbol{\theta})$. The procedure of adapting the many-body wavefunction and orbital refinement is then repeated sequentially until the energy converges to a given threshold. We illustrate our proposed multiresolution quantum computing framework in the flow chart depicted in Fig. 1.

In passing, we note that our proposed workflow bears a close resemblance to the Complete Active Space Self-Consistent Field (CASSCF) approach commonly used in quantum chemistry, in which both the many-body wavefunction and the orbitals are optimized in a similar fashion. In contrast to CASSCF and the use of (Gaussian-type atom-centered) basis sets, our orbital refinement step is not limited to the space spanned by the basis functions, which means that unmatched results can be obtained with the same number of orbitals. To this end, we are discriminating between orbital optimization—rotating the current set of active orbitals within the given orbital basis, and orbital refinement, where the orbital basis gets refined with the methodology described above. As with orbital optimization, orbital refinement with MRA orbitals can be combined with any other quantum chemistry method, which allows the calculation of RDMs, for example, coupled cluster methods, configuration interaction, or tensor-network approaches such as DMRG.

IV. NUMERICAL DEMONSTRATIONS

Subsections IV A–IV D summarize numerical demonstrations of our proposed multiresolution quantum framework described in Sec. III on selected test systems. We commence with one of the largest possible systems for the orbital refinement implementation presented in this work, cyclohexane with 36 active electrons in 36 spatial (72 spin-) orbitals. Subsequently, we highlight the fundamental features of orbital refinement compared to the previous PNO approximation on simple (effective) two-electron model systems (H_2 and LiH) before continuing with chemically more interesting systems (BeH_2 and H_4). In the latter, we will in particular highlight the influence of an approximate VQE *Ansatz* (leading to a qubit wavefunction with varying quality across the molecular instances) on the basis refinement.

In Table I, we summarize the notation used within this work. It follows the standard pattern: WFN/BASIS(N_e, N_q), where WFN refers to the method employed to represent the second quantized many-electron wavefunction (or quantum circuit) and BASIS refers to the method employed to determine the one-electron basis functions (spatial orbitals) that define the second quantized Hamiltonian (5). The numbers N_e and N_q refer to the number of active electrons and qubits, respectively (the latter being equal to the number of spin-orbitals) for our multi-configurational wavefunction *Ansatz*.

For standard Gaussian basis sets, BASIS is just the identifier of the corresponding basis set. For example, FCI/cc-pVDZ(N_e, N_q) denotes a full CI calculation, that is, an exact diagonalization in

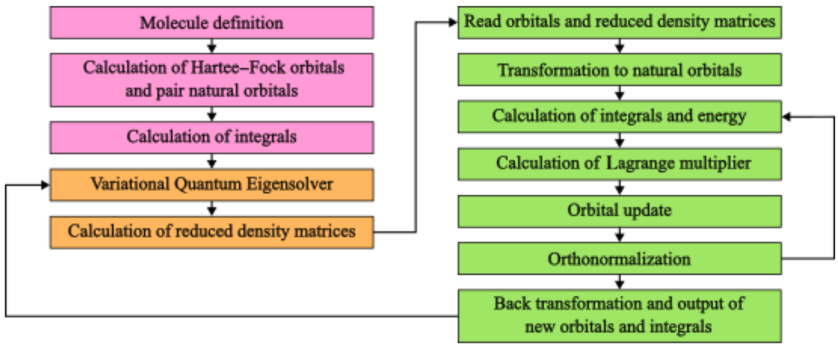

FIG. 1. Flow chart of the proposed multiresolution quantum framework. Based on initial HF orbitals and pair natural orbitals as well as their integrals with the molecular Hamiltonian (pink), energy and RDMs are determined using a VQE *Ansatz* (orange) alternating with an orbital refinement step (green).

16 October 2026 14:53:26

© Author(s) 2026

TABLE I. Notation: Methods are denoted as WFN/BASIS(N_e, N_s), where WFN denotes the method to describe the many-body wavefunction (e.g., SPA+GSD, FCI, and CASSCF), while BASIS denotes the various orbital bases listed in this table. See Sec. IV for some examples.

Basis identifiers	Details
PNO	Short for MRA-PNO as in Ref. 15
MRA	Orbitals refined as in Sec. III
MRA[it=n]	Results after n macro-iterations
MRA[opt=n]	Only the first n orbitals are refined
MRA[wfn=X]	Different wavefunctions used for refinement
(aug-)cc-pVXZ	Reference Gaussian basis sets [82]

the N_e-electron singlet subspace, and N_q will refer to two times the number of basis orbitals in the standard basis set cc-pVDZ (corresponding to the number of qubits in most encodings). By contrast, for MRA represented orbitals, we use the general notation: MRA[wfn, opt, it], where "wfn" denotes the many-electron wavefunction used in the basis refinement, "opt" denotes the number of orbitals that are refined, and "it" denotes the number of macro-iterations. For better readability, we list in Table I all abbreviations of this general format.

In the supplementary material, we provide further computational details for the numerical studies in this work along with references to the employed software packages.

A. Cyclohexane

We used the cyclohexane molecule as a demonstration of a molecule that is still feasible to compute with the exact basis refinement and will give an exemplary illustration of the cost and perspective gains of orbital refinement. The results are shown in Fig. 2. To the best of our knowledge, this is one of the largest simulations for VQE optimizations as well as exact orbital determination.

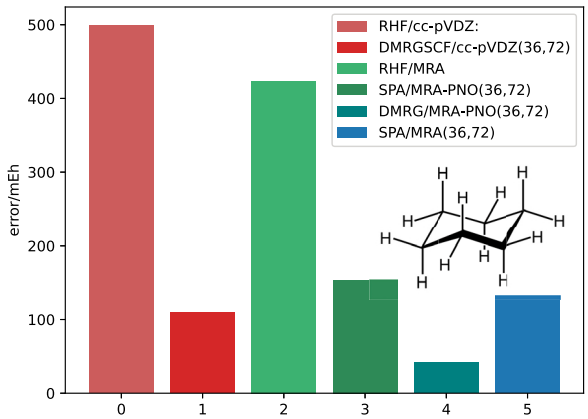

FIG. 2. Applicability: Full calculation of the cyclohexane molecule in an active space of 36 electrons and 36 spatial (72 spin) orbitals with different orbitals and many-body methods. This serves as a stand-in for the system sizes still treatable with the method. We show the energy difference (atomic units) with respect to DMRG[BD=1000]/MRA(36,72). In this example, MRA-PNOs are computationally cheapest while still comparable in numerical precision.

In the example, we use DMRG/[BD=1000]MRA(36,72) to determine the optimal minimal basis for this molecule. We then compare combinations of DMRG, SPA many-body wavefunctions combined with MRA-PNOs or fully refined orbital bases with varying many-body methods used for the determination. When compared to the cheaper MRA-PNOs, the total error is between 20 and 40 mEh, depending on the used many-body state: in this case, either a SPA quantum circuit or a DMRG calculation with large bond dimension. The determination of the MRA-PNOs takes around 15 min on a standard compute node, while the full refinement coupled to a DMRG calculation takes around 1–2 days. These timings should not be taken as accurate benchmarks but rather as illustrations of the necessary cost to reach the last 20–40 mEh in the energy. In this case, a full basis refinement with quantum circuits on SPA level alone is most likely not an attractive scenario, as the method-error of the SPA circuits alone is already around 100 mEh, which is significantly higher as the corresponding basis error of around 20 mEh.

To put the numbers into perspective: An orbital-optimized active space simulation within the cc-pVDZ basis already has a significantly larger basis error of around 100 mEh (75 of them already at the mean-field level). In our case, the calculation took around 15 h and was significantly longer than the MRA-PNOs that took around 15 min (with around the same time for the subsequent many-body simulation).

B. H_2 and LiH

To study the influence of orbital optimization on the energy and the many-body wavefunction, we calculated the dissociation curves of H_2 and LiH with different active spaces. For both molecules, SPA circuits can describe the (effective) two-electron systems exactly if the orbitals are in the correct linear combination.[78] We use a slightly expanded approach in the form of SPA+GSD (SPA plus a layer of generalized pair-excitations that are missing in the leading SPA excitations, followed by a layer of generalized singles excitations) to aid the orbital-optimizer in finding the correct linear combinations.

To verify whether and how fast the orbitals and the multi-particle wavefunction expressed by reduced density matrices converge with alternating optimization, the dissociation curve of H_2 with four spin-orbitals was considered as the simplest possible test case with results displayed in Fig. 3. In the case of the dissociated H_2, the system is resolved exactly with two spatial orbitals given by the analytic solution of the isolated hydrogen atom. The spatial orbital basis determined via the MP2-PNO model is not able to represent this solution due to the neglect of important coupling terms in the MP2 model. Hence, a refinement of the PNO basis via Eq. (33) is able to correct this deficiency in a single iteration. By comparison, at shorter bond distances, the energy of the refined basis is of similar quality as the CASSCF/aug-cc-pVTZ(2,4) reference, which indicates that this is the best possible representation restricted to two spatial orbitals only, and the resulting error is solely due to this restriction. We confirm the latter hypothesis by increasing the number of spatial orbitals in the active space from 2 to 9. As illustrated in Fig. 3, this modest increase results in a smooth convergence toward the full FCI/aug-cc-pVTZ(2,92) energy (obtained with 46 orbitals). In passing, we note that the remaining total error is lower than 3 mhartree compared to an aug-cc-pV5Z reference,

16 October 2026 14:53:26

© Author(s) 2026

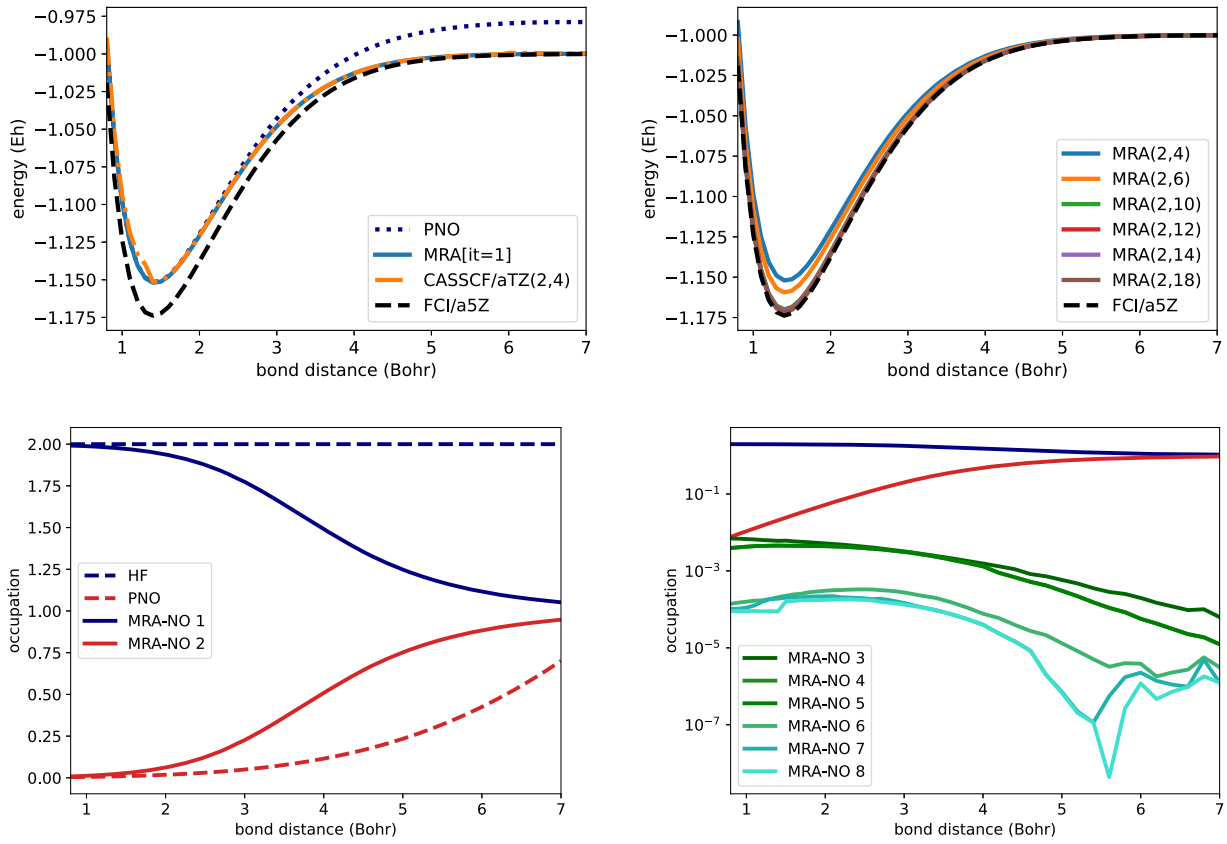

FIG. 3. Illustration on the H_2 molecule: Comparison of the H_2 dissociation calculated with SPA+GSD(2,4) and adaptive MRA orbitals after several optimization steps starting from pair natural orbitals as an initial guess. Top row: total energies. Bottom row: occupation numbers.

indicating that we can essentially reach the basis set limit for this system.

The convergence behavior in the case of the H_2 molecule can be explained as follows: In a representation with two spatial natural orbitals ϕ_0 and ϕ_1, the full first-quantized wavefunction of H_2 can be expressed as a linear combination of two anti-symmetric pair functions,

$$\Psi_{00} = \phi_0(r_1)\phi_0(r_2) \otimes S(s_1, s_2), \tag{36}$$

$$S(s_1, s_2) = \frac{1}{\sqrt{2}}(|\uparrow\downarrow\rangle - |\downarrow\uparrow\rangle), \tag{37}$$

and similarly for Ψ_{11}. The total wavefunction can then be written as

$$\Psi = c_0\Psi_{00} + c_1\Psi_{11} \tag{38}$$

with the energy expectation value

$$E = \langle\Psi|H|\Psi\rangle = c_0^2\langle\Psi_{00}|H|\Psi_{00}\rangle + 2c_0c_1\langle\Psi_{00}|H|\Psi_{11}\rangle + c_1^2\langle\Psi_{11}|H|\Psi_{11}\rangle. \tag{39}$$

The initial orbitals obtained with an MP2-PNO approach essentially assume $c_0 \gg c_1$—the total wavefunction is dominated by a single configuration Ψ_{00}, whereas Ψ_{11} is just a small perturbation. The ϕ_0 is then determined through the minimization of $\langle\Psi_{00}|H|\Psi_{00}\rangle$ alone (Hartree–Fock), while ϕ_1 is determined by keeping only first-order terms (in the two-body interaction) in c_1, hence disregarding most of $c_1^2\langle\Psi_{11}|H|\Psi_{11}\rangle$. If the underlying assumption $c_0 \gg c_1$ holds, this is physically justified; in the dissociated case, we have, however, $c_0 = c_1$, leading to an unbalanced treatment in the determination of both orbitals—as a result of neglecting the coupling between ϕ_1 and ϕ_0 in the determination of Ψ_{00} and the coupling between ϕ_1 and ϕ_0 in the determination of Ψ_{11}.

In Fig. 4, a similar behavior can be observed for LiH. Here, the total errors are larger as we are dealing with a more correlated system, although the dissociated LiH still contains only two active electrons. In LiH, we assumed a frozen core approximation, keeping the two core ($1s$) electrons of the Li atom frozen in all calculations. For a discussion on the validity of this approximation even for orbital bases that allow core correlation, see the Appendix of Ref. 78.

As an alternative to enlarging the active space and optimizing all orbitals, only a limited number of active orbitals can be optimized as the active space increases. This possibility was also investigated using a (2, 18) active space for H_2 and a (2, 16) active space for LiH (see Fig. 4). Here, only a fixed number of initial NOs (ordered by their respective occupation numbers) are refined.

16 October 2026 14:53:26

© Author(s) 2026

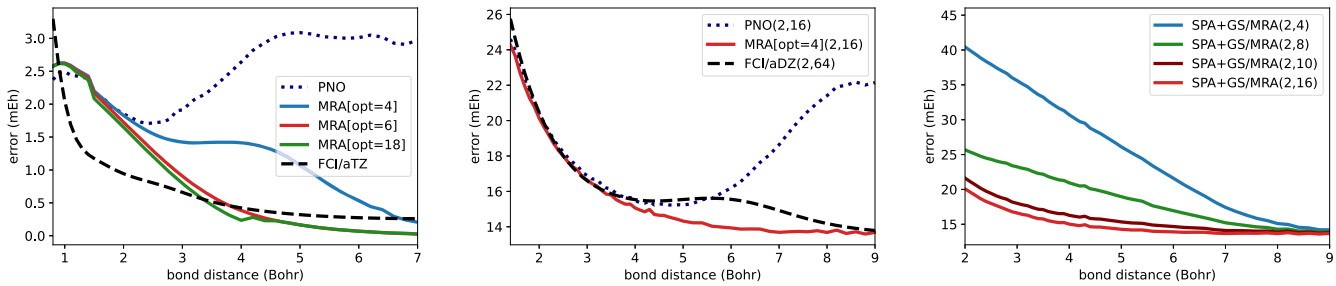

FIG. 4. Effect of selective refinement: Orbitals of an initial orbital set (in the form of PNOs) are gradually refined, while the others remain in their initial form (up to orthogonalization effects). Left: Absolute errors with respect to FCI/aug-cc-pV5Z for H_2. Center: Absolute errors with respect to FCI/aug-cc-pVQZ for LiH. Right: Absolute errors of LiH (same reference values), but here the number of fully refined MRA orbitals is gradually increased. The red line, SPA+GS/MRA(2,18), is identical to the plot in the center. For H_2 (left), the difference of the reference values to the next basis set (aug-cc-pV5Z) is consistently below the millihartree threshold. For LiH, aug-cc-pVTZ was chosen as a reference as it contains a similar amount of orbitals on Li as aug-cc-pVQZ on H.

The examples illustrate that it is not always necessary to refine all initial orbitals, and thus, the computational cost of the refinement can potentially be reduced. In our current implementation, a limitation to a fixed number of orbitals does, however, not result in considerable savings in computational time. Furthermore, orbitals that are not optimized are also modified in each optimization cycle to ensure orthonormalization, which entails that the one- and two-electron integrals of these orbitals must also be updated in each cycle nonetheless—and this step can become computationally quite expensive.

C. BeH_2

As a further example, we studied the dissociation of BeH_2 by means of SPA+GSD/MRA and CASSCF calculations employing active spaces of different sizes. In contrast to H_2 and LiH, BeH_2 has four valence electrons such that the SPA+GSD approach is no longer exact by construction, which allows us to study the effects of an imperfect *Ansatz* on the refinement of the orbital basis. The dissociation curves with all three methods for the active spaces (4, 8), (4,12), and (4,16) are summarized in Fig. 5.

A comparison of SPA+GSD/MRA with FCI/MRA shows that the SPA+GSD approach can reproduce the FCI/MRA energy almost exactly for all active spaces, both around the equilibrium distance and for high distances in a dissociated situation. This can be explained on the basis of valence-bond resonance structures, where the "molecular" one dominates around the equilibrium, while the "atomic" resonance structure dominates at the dissociated limit. An SPA *Ansatz* can represent only a single resonance structure, so its associated error will decrease within the dissociation curve. For a further in-depth discussion, we refer the interested reader to Ref. 79, in particular Fig. 5 and its accompanying text therein.

Turning next to a comparison of FCI/MRA with CASSCF/aug-cc-pVTZ shows a consistent behavior of the refined bases with respect to its traditional counterpart. In passing, we note a challenging convergence of the smallest active space for the CASSCF with default parameters (PYSCF implementation), which can be attributed to a convergence to local minima often encountered for large and diffuse Gaussian basis sets like the one we employ in the current case (aug-cc-pVTZ). Convergence to local minima could then be avoided if one employs active-space selection tools like the ones detailed, for example, in Refs. 7 and 9, respectively.

D. H_4

As a final example, we will study the potential energy surface for the Paldus[83] $H_4/(H_2)_2$ system. Similar to BeH_2, the SPA *Ansatz* is unable to describe the full potential energy surface with the same accuracy, leading to a cusp-like feature in the resulting energy error around the square structure. The underlying reason

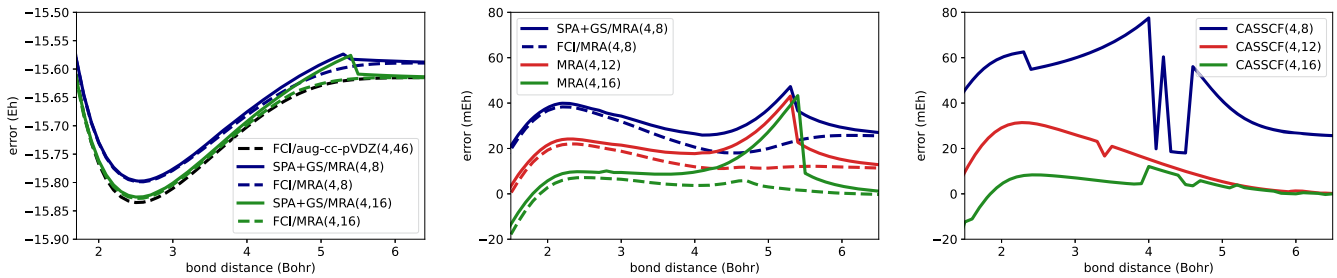

FIG. 5. BeH_2 in MRA orbitals determined by VQEs (SPA+GS). Left: Absolute energies. Center: Energy errors relative to FCI/cc-pVDZ(4,46). Right: CASSCF/aug-cc-pVTZ with different sizes labeled as $(N_e, 2N_o)$ using the number of spin-orbitals $2N_o$ for consistency in notation.

16 October 2026 14:53:26

© Author(s) 2026

comes from the inability of the SPA *Ansatz* to describe more than a single valence-bond resonance structure, while the square configuration has two degenerate resonance structures.[79] The system here was specifically selected because of this shortcoming of the quantum circuit. SPA+GSD/MRA, FCI/MRA, and CASSCF calculations were performed with the active spaces (4,8), (4,12), (4,16), and (4,20) with the potential energy curves around the square configuration, and the results are summarized in Fig. 6. Regardless of the method, a significant reduction in the energy over the entire potential energy curve can be seen with increasing active spaces. Notably, the energy does not yet appear to converge with the active space size even for the largest active spaces. As expected, the deviation in energy is particularly large around the square configuration, as more orbitals are required to correctly describe the increasingly complex chemical bonding situation.

Overall, MRA methods provide continuous energy profiles and almost consistently lower energies than the CASSCF counterpart, where significant energy jumps occur in some cases, highlighting difficulties in converging the CAS wavefunction without manual (or automated) adjustment of the CAS space orbitals. A comparison between SPA+GSD calculations with non-optimized orbitals (SPA+GSD/PNO) and optimized orbitals (SPA+GSD/MRA) shows hardly any differences at the example of the (4,20) active space, indicating that the HF orbitals and PNOs were already almost optimal for the problem at hand. If the SPA+GSD solver is replaced by FCI based on the previously optimized SPA+GSD/MRA orbitals (FCI/MRA[wfn=SPA+GSD]), lower energies are obtained, although the kink in the quadratic configuration remains albeit slightly mitigated. This finding indicates that the shortcomings of the SPA *Ansatz* were inherited with the refined basis in a more drastic way, as, for example, with the BeH_2 molecule.

When switching to an FCI based refinement, there is still an observable deficiency around the square configuration where the energetic lowering with increasing basis set size seems to be hindered. The visualization of the active orbitals after orbital optimization provides insights into the reason for this behavior. For H_4 in the square configuration with a (4, 16) active space, all active spatial orbitals before optimization, including their PNO occupation,

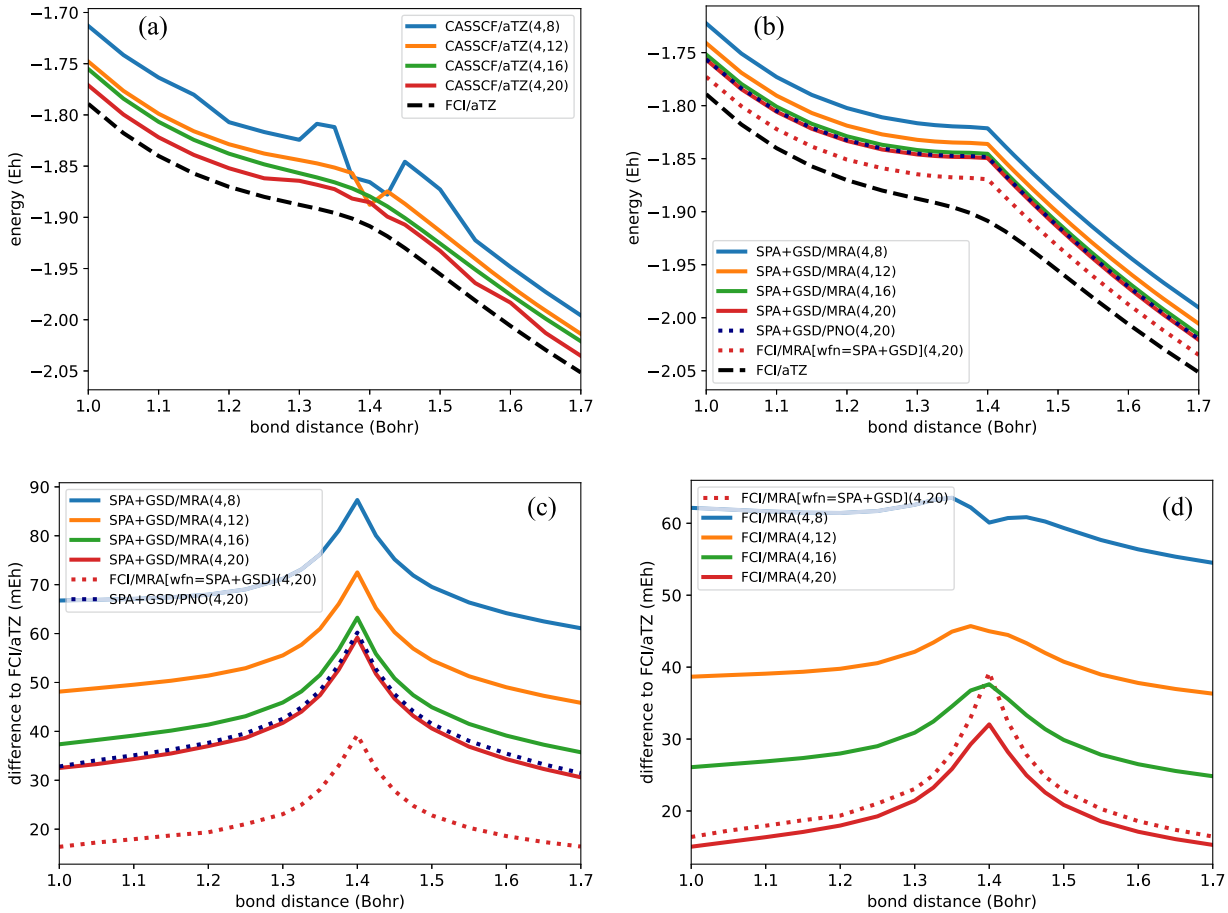

FIG. 6. Comparison of methods for H_4: Comparison between CASSCF/aug-cc-pVTZ (a) with SPA+GSD [(b) and (c)], and FCI (d) each with optimized MRA orbitals for the dissociation of two parallel hydrogen molecules for different active spaces. All calculations use PNOs (see Fig. 7) as initial guesses.

16 October 2026 14:53:26

© Author(s) 2026

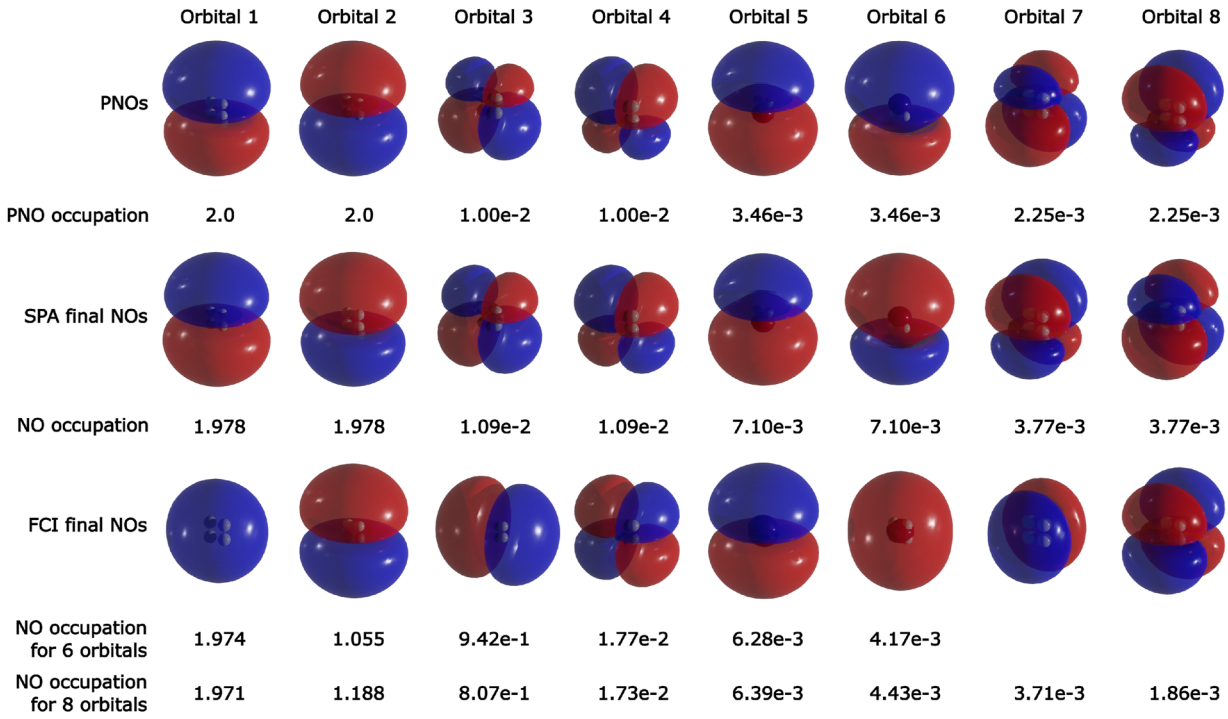

FIG. 7. MRA orbitals for H_4: Initial HF orbitals and PNOs as well as the optimized natural orbitals and their occupation resulting from a SPA+GSD or FCI calculation with 2 active electrons in 8 (6) spatial orbitals for a quadratic H_4 configuration.

as well as the NOs optimized with SPA+GSD/MRA and FCI/MRA, including occupation numbers, are depicted in Fig. 7.

With the exception of phase changes and the exchange of the order of equally occupied orbitals, there are no significant differences between the original PNOs and the final NOs from the MRA-SPA calculation. Although the orbitals were refined and the energy lowered, SPA is not able to describe the binding situation correctly. In SPA, the system is treated as two parallel H_2 molecules with one bond each, and thus, only one of the two possible resonance structures is described accurately. This limitation is particularly evident in the NO populations. Thus, one set of four orbitals is obtained for each H_2 bond, with the NOs having the same populations for both bonds. By contrast, FCI-MRA can describe both resonance structures simultaneously and thus the many-body wavefunction correctly. As a result, the orbital shape also changes fundamentally in the refinement process, and the populations of orbitals 2 and 3 approach each other (last row in Fig. 7). Ideally, both orbitals should have the same population after the refinement, but in the case of a six-orbital calculation, the energy converges before both orbitals have exactly the same shape and population. In the case of a calculation with eight orbitals, the two additionally generated PNOs favor one of the two resonance structures, which eliminates the expected degeneracy of the ground state, and the populations of orbitals 2 and 3 do not equalize any further. This physically inaccurate description cannot be compensated for by the orbital refinement, as it is not able to break certain symmetries. The selection of suitable initial orbitals via PNOs, therefore, represents a limitation in the method presented here and requires particular attention in challenging cases such as H_4. Interpretive concepts based on valence-bond resonance structures[78,79] provide a valuable tool in estimating these effects.

V. CONCLUSION AND OUTLOOK

In this work, we have presented a novel approach for quantum chemistry in the framework of quantum computing that combines variational quantum eigensolvers with a basis-free representation of orbitals. Starting from initial MRA representations of Hartree–Fock orbitals and PNOs, the chosen VQE *Ansatz* is alternately re-optimized, and a refinement of the orbitals is performed until both parts converge. The resulting orbitals, dependent on the initial guess, thus obtained provide the best possible energies, while at the same time *eliminating the need* to choose a basis set. Furthermore, the use of PNOs provides a systematic basis to define active spaces and avoids a time-consuming selection of a suitable and system-dependent space. In the numerical examples of this work, they provide well-suited initial guesses for the full refinement on a broad range of molecules, where we highlighted and analyzed exceptions and potential shortcomings of PNO guesses. The capability to calculate the best possible energy from a given number of orbitals without including unnecessary orbitals in the active space allows in most cases a reduction in the active space size without significant loss of accuracy and thus reduces the number of required qubits and gates in the case of VQEs. All these advantages, but also current

16 October 2026 14:53:26

© Author(s) 2026

limitations, were demonstrated by combining orbital refinement with the SPA+GSD VQE *Ansatz* using various electron correlation and chemical bonding challenges at the example of a number of textbook molecular systems for quantum-chemistry developments. In most cases, our VQE approach with refined orbitals led to consistently better and, above all, continuous energies over the entire dissociation profiles compared to (unguided) CASSCF reference calculations in large basis sets. From a quantum computing point of view, all examples discussed in this work exemplify how results obtained with a VQE *Ansatz* based on MRA-PNOs can be improved without modifying the *Ansatz* itself, making the *Ansatz* with its low circuit depth a promising candidate for meaningful quantum chemistry calculations on real, contemporary quantum hardware.

Even though the code for orbital refinement developed in this work stands on the shoulders of the high-performance library MADNESS,[27] it is not yet fully optimized, which means that the number of possible orbitals is lower than it could be. Nevertheless, the code is suitable for making use of significantly larger active spaces than those demonstrated in this work. Work along these lines is currently in progress and will be published elsewhere. Notably, the initial MRA-PNO code can, for example, already be routinely employed to compute systems with hundreds of orbitals.[13] In the foreseeable future, the limiting factor is, therefore, the solution of the many-particle wavefunction and the simulation/execution of/on a quantum computer. Furthermore, we would like to point out that the combination of orbital refinement with an initial active space comprised of PNOs as demonstrated in this work as well as the newly developed code base is not limited to the use of VQEs but can also effortlessly be combined with other classical active space solvers.[16]

SUPPLEMENTARY MATERIAL

See the supplementary material for further details on the used computational methods.

ACKNOWLEDGMENTS

J.S.K. acknowledges funding from the Hightech Agenda of the state of Bavaria and the German Federal Ministry of Research, Technology and Space (BMFTR) via Quantum Technologies:HoliQC2. This work in-part used the resources on the LiCCA HPC cluster of the University of Augsburg, co-funded by the Deutsche Forschungsgemeinschaft (DFG, German Research Foundation), Project No. 499211671. The idea for this work was born at the "Numerical Methods in Quantum Chemistry" workshop 2023 in Tromsø, Norway. S.K. and J.S.K. would, therefore, like to thank the organizers for a truly inspiring conference in an astonishing setting beyond the northern Arctic Circle. S.K. and F.L. furthermore acknowledge fruitful discussions with Roberto di Remigio Eikås and Leander Thiessen.

AUTHOR DECLARATIONS

Conflict of Interest

The authors have no conflicts to disclose.

Author Contributions

Fabian Langkabel: Conceptualization (equal); Data curation (equal); Formal analysis (equal); Investigation (equal); Methodology (equal); Project administration (equal); Resources (equal); Software (equal); Validation (equal); Visualization (equal); Writing – original draft (equal); Writing – review & editing (equal). **Stefan Knecht**: Conceptualization (equal); Project administration (equal); Resources (equal); Supervision (equal); Writing – original draft (supporting); Writing – review & editing (equal). **Jakob S. Kottmann**: Conceptualization (equal); Data curation (equal); Formal analysis (equal); Funding acquisition (equal); Investigation (equal); Methodology (equal); Project administration (equal); Resources (equal); Software (equal); Supervision (equal); Validation (equal); Visualization (equal); Writing – original draft (equal); Writing – review & editing (equal).

DATA AVAILABILITY

The data that support the findings will be available in the FrayedEnds repository on GitHub at https://github.com/FabianLangkabel/FrayedEnds/ following an embargo from the date of publication to allow for commercialization of research findings.

REFERENCES

[1] A. Aspuru-Guzik, A. D. Dutoi, P. J. Love, and M. Head-Gordon, "Simulated quantum computation of molecular energies," Science **309**, 1704 (2005).
[2] M. Reiher, N. Wiebe, K. M. Svore, D. Wecker, and M. Troyer, "Elucidating reaction mechanisms on quantum computers," Proc. Natl. Acad. Sci. U. S. A. **114**, 7555 (2017).
[3] V. von Burg, G. H. Low, T. Häner, D. S. Steiger, M. Reiher, M. Roetteler, and M. Troyer, "Quantum computing enhanced computational catalysis," Phys. Rev. Res. **3**, 033055 (2021).
[4] D. Rocca, C. L. Cortes, J. F. Gonthier, P. J. Ollitrault, R. M. Parrish, G.-L. Anselmetti, M. Degroote, N. Moll, R. Santagati, and M. Streif, "Reducing the runtime of fault-tolerant quantum simulations in chemistry through symmetry-compressed double factorization," J. Chem. Theory Comput. **20**, 4639 (2024).
[5] C. J. Stein and M. Reiher, "AUTOCAS: A program for fully automated multiconfigurational calculations," J. Comput. Chem. **40**, 2216 (2019).
[6] M. Bensberg, M. Mörchen, C. J. Stein, J. P. Unsleber, T. Weymuth, and M. Reiher, qcscine/autocas: Release 2.1. 0 (2023).
[7] C. J. Stein and M. Reiher, "Automated selection of active orbital spaces," J. Chem. Theory Comput. **12**, 1760 (2016).
[8] C. J. Stein, V. von Burg, and M. Reiher, "The delicate balance of static and dynamic electron correlation," J. Chem. Theory Comput. **12**, 3764 (2016).
[9] E. R. Sayfutyarova, Q. Sun, G. K.-L. Chan, and G. Knizia, "Automated construction of molecular active spaces from atomic valence orbitals," J. Chem. Theory Comput. **13**, 4063 (2017).
[10] L. Ding, S. Knecht, and C. Schilling, "Quantum information–assisted complete active space optimization (QICAS)," J. Phys. Chem. Lett. **14**, 11022 (2023).
[11] A. Mitra, R. D'Cunha, Q. Wang, M. R. Hermes, Y. Alexeev, S. K. Gray, M. Otten, and L. Gagliardi, "The localized active space method with unitary selective coupled cluster," J. Chem. Theory Comput. **20**(18), 7865–7875 (2024).
[12] F. Tarocco, P. A. B. Haase, F. Pavošević, V. Krishna, L. Guidoni, S. Knecht, and M. Stella, "AEGISS – Atomic orbital and entropy-based guided inference for space selection – A novel semi-automated active space selection workflow for quantum chemistry and quantum computing applications," arXiv:2508.10671 (2025).
[13] J. S. Kottmann, F. A. Bischoff, and E. F. Valeev, "Direct determination of optimal pair-natural orbitals in a real-space representation: The second-order Moller–Plesset energy," J. Chem. Phys. **152**, 074105 (2020).

16 October 2026 14:53:26

© Author(s) 2026

[14]J. S. Kottmann, P. Schleich, T. Tamayo-Mendoza, and A. Aspuru-Guzik, "Reducing qubit requirements while maintaining numerical precision for the variational quantum eigensolver: A basis-set-free approach," J. Phys. Chem. Lett. **12**, 663 (2021).
[15]J. S. Kottmann and A. Aspuru-Guzik, "Optimized low-depth quantum circuits for molecular electronic structure using a separable-pair approximation," Phys. Rev. A **105**, 032449 (2022).
[16]E. F. Valeev, R. J. Harrison, A. A. Holmes, C. C. Peterson, and D. A. Penchoff, "Direct determination of optimal real-space orbitals for correlated electronic structure of molecules," J. Chem. Theory Comput. **19**, 7230 (2023).
[17]M. Nibbi, L. Frediani, E. Dinvay, and C. B. Mendl, "Wavefunction optimization at the complete basis set limit with multiwavelets and DMRG," J. Phys. Chem. A **129**(47), 11041–11052 (2025).
[18]P. Haubenwallner and M. Heller, "Fully numerical Hartree-Fock calculations for atoms and small molecules with quantics tensor trains," Electron. Struct. **7**, 025006 (2025).
[19]C.-L. Hong, T. Tsai, J.-P. Chou, P.-J. Chen, P.-K. Tsai, Y.-C. Chen, E.-J. Kuo, D. Srolovitz, A. Hu, Y.-C. Cheng, and H.-S. Goan, "Accurate and efficient quantum computations of molecular properties using Daubechies wavelet molecular orbitals: A benchmark study against experimental data," PRX Quantum **3**, 020360 (2022).
[20]L. Genovese, B. Videau, M. Ospici, T. Deutsch, S. Goedecker, and J.-F. Méhaut, "Daubechies wavelets for high performance electronic structure calculations: The BigDFT project, C. R. Méc. **339**, 149 (2011).
[21]T. Tamayo-Mendoza, C. Kreisbeck, R. Lindh, and A. Aspuru-Guzik, "Automatic differentiation in quantum chemistry with applications to fully variational Hartree–Fock," ACS Cent. Sci. **4**, 559 (2018).
[22]J. M. Arrazola, S. Jahangiri, A. Delgado, J. Ceroni, J. Izaac, A. Száva, U. Azad, R. A. Lang, Z. Niu, O. Di Matteo *et al.*, "Differentiable quantum computational chemistry with PennyLane," arXiv:2111.09967 (2021).
[23]X. Zhang and G. K.-L. Chan, "Differentiable quantum chemistry with PySCF for molecules and materials at the mean-field level and beyond," J. Chem. Phys. **157**, 204801 (2022).
[24]P. J. Ollitrault, J. F. Gonthier, D. Rocca, G.-L. Anselmetti, M. Degroote, N. Moll, R. Santagati, and M. Streif, "Improving the runtime of quantum phase estimation for chemistry through basis set optimization," J. Chem. Theory Comput. **21**(23), 12034–12047 (2025).
[25]M. F. Herbst, "Development of a modular quantum-chemistry framework for the investigation of novel basis functions," Ph.D. thesis, Ruprecht-Karls-Universität Heidelberg, 2018.
[26]P. Jordan and O. Klein, "Zum mehrkörperproblem der quantentheorie," Z. Phys. **45**, 751 (1927).
[27]R. J. Harrison, G. Beylkin, F. A. Bischoff, J. A. Calvin, G. I. Fann, J. Fosso-Tande, D. Galindo, J. R. Hammond, R. Hartman-Baker, J. C. Hill *et al.*, "MADNESS: A multiresolution, adaptive numerical environment for scientific simulation," SIAM J. Sci. Comput. **38**, S123 (2016).
[28]P. Wind, M. Bjørgve, A. Brakestad, G. A. Gerez S, S. R. Jensen, R. D. R. Eikås, and L. Frediani, "MRChem multiresolution analysis code for molecular electronic structure calculations: Performance and scaling properties," J. Chem. Theory Comput. **19**, 137 (2022).
[29]M. Bjørgve, C. Tantardini, S. R. Jensen, G. A. Gerez S, P. Wind, R. Di Remigio Eikås, E. Dinvay, and L. Frediani, "VAMPyR—A high-level Python library for mathematical operations in a multiwavelet representation," J. Chem. Phys. **160**, 162502 (2024).
[30]R. J. Harrison, G. I. Fann, T. Yanai, Z. Gan, and G. Beylkin, "Multiresolution quantum chemistry: Basic theory and initial applications," J. Chem. Phys. **121**, 11587 (2004).
[31]T. Yanai, G. I. Fann, Z. Gan, R. J. Harrison, and G. Beylkin, "Multiresolution quantum chemistry in multiwavelet bases: Hartree–Fock exchange," J. Chem. Phys. **121**, 6680 (2004).
[32]S. R. Jensen, A. Durdek, M. Bjørgve, P. Wind, T. Flå, and L. Frediani, "Kinetic energy-free Hartree–Fock equations: An integral formulation," J. Math. Chem. **61**, 343 (2023).
[33]F. A. Bischoff, R. J. Harrison, and E. F. Valeev, "Computing many-body wave functions with guaranteed precision: The first-order Møller-Plesset wave function for the ground state of helium atom," J. Chem. Phys. **137**, 104103 (2012).
[34]F. A. Bischoff and E. F. Valeev, "Computing molecular correlation energies with guaranteed precision," J. Chem. Phys. **139**, 114106 (2013).
[35]J. S. Kottmann and F. A. Bischoff, "Coupled-cluster in real space. 1. CC2 ground state energies using multiresolution analysis," J. Chem. Theory Comput. **13**, 5945 (2017).
[36]J. S. Kottmann and F. A. Bischoff, "Coupled-cluster in real space. 2. CC2 excited states using multiresolution analysis," J. Chem. Theory Comput. **13**, 5956 (2017).
[37]J. S. Kottmann, "Coupled-cluster in real space," Ph.D. thesis, Humboldt-Universität zu Berlin, Mathematisch-Naturwissenschaftliche Fakultät, 2018.
[38]S. Barison, D. E. Galli, and M. Motta, "Quantum simulations of molecular systems with intrinsic atomic orbitals," Phys. Rev. A **106**(2), 022404 (2022).
[39]J. R. McClean, F. M. Faulstich, Q. Zhu, B. O'Gorman, Y. Qiu, S. R. White, R. Babbush, and L. Lin, "Discontinuous Galerkin discretization for quantum simulation of chemistry," New J. Phys. **22**, 093015 (2020).
[40]S. R. Jensen, S. Saha, J. A. Flores-Livas, W. Huhn, V. Blum, S. Goedecker, and L. Frediani, "The elephant in the room of density functional theory calculations," J. Phys. Chem. Lett. **8**, 1449 (2017).
[41]A. Hurtado, H. Sekino, and R. J. Harrison, "Benchmarking correlation-consistent basis sets for frequency-dependent polarizabilities with multiresolution analysis," J. Chem. Theory Comput. **20**, 5145 (2024).
[42]Q. Pitteloud, P. Wind, S. R. Jensen, L. Frediani, and F. Jensen, "Quantifying intramolecular basis set superposition errors," J. Chem. Theory Comput. **19**, 5863 (2023).
[43]J. B. Stückrath and F. A. Bischoff, "Reduction of Hartree–Fock wavefunctions to Kohn–Sham effective potentials using multiresolution analysis," J. Chem. Theory Comput. **17**, 1408 (2021).
[44]T. Yanai, R. J. Harrison, and N. C. Handy, "Multiresolution quantum chemistry in multiwavelet bases: Time-dependent density functional theory with asymptotically corrected potentials in local density and generalized gradient approximations," Mol. Phys. **103**, 413 (2005).
[45]N. Poirier, J. S. Kottmann, A. Aspuru-Guzik, L. Mongeau, and A. Najafi-Yazdi, "Range-separated density functional theory using multiresolution analysis and quantum computing," J. Comput. Chem. **45**, 1987 (2024).
[46]S. R. Jensen, T. Flå, D. Jonsson, R. S. Monstad, K. Ruud, and L. Frediani, "Magnetic properties with multiwavelets and DFT: The complete basis set limit achieved," Phys. Chem. Chem. Phys. **18**, 21145 (2016).
[47]F. A. Bischoff, "Structure of the H_3 molecule in a strong homogeneous magnetic field as computed by the Hartree-Fock method using multiresolution analysis," Phys. Rev. A **101**, 053413 (2020).
[48]A. Brakestad, S. R. Jensen, P. Wind, M. D'Alessandro, L. Genovese, K. H. Hopmann, and L. Frediani, "Static polarizabilities at the basis set limit: A benchmark of 124 species," J. Chem. Theory Comput. **16**, 4874 (2020).
[49]R. Cammi, L. Frediani, B. Mennucci, J. Tomasi, K. Ruud, and K. V. Mikkelsen, "A second-order, quadratically convergent multiconfigurational self-consistent field polarizable continuum model for equilibrium and nonequilibrium solvation," J. Chem. Phys. **117**, 13 (2002).
[50]G. A. Gerez S, R. Di Remigio Eikås, S. R. Jensen, M. Bjørgve, and L. Frediani, "Cavity-free continuum solvation: Implementation and parametrization in a multiwavelet framework," J. Chem. Theory Comput. **19**, 1986 (2023).
[51]J. Anderson, B. Sundahl, R. Harrison, and G. Beylkin, "Dirac-Fock calculations on molecules in an adaptive multiwavelet basis," J. Chem. Phys. **151**, 234112 (2019).
[52]J. Anderson, R. J. Harrison, B. Sundahl, W. S. Thornton, and G. Beylkin, "Real-space quasi-relativistic quantum chemistry," Comput. Theor. Chem. **1175**, 112711 (2020).
[53]A. Brakestad, S. R. Jensen, C. Tantardini, Q. Pitteloud, P. Wind, J. Užulis, A. Gulans, K. H. Hopmann, and L. Frediani, "Scalar relativistic effects with multiwavelets: Implementation and benchmark," J. Chem. Theory Comput. **20**, 728 (2024).
[54]C. Tantardini, R. Di Remigio Eikås, M. Bjørgve, S. R. Jensen, and L. Frediani, "Full Breit Hamiltonian in the multiwavelets framework," J. Chem. Theory Comput. **20**, 882 (2024).
[55]R. D. Remigio, M. Repisky, S. Komorovsky, P. Hrobarik, L. Frediani, and K. Ruud, "Four-component relativistic density functional theory with the polarisable continuum model: Application to EPR parameters and paramagnetic NMR shifts," Mol. Phys. **115**, 214 (2017).

16 October 2026 14:53:26

© Author(s) 2026

[56]J. Anderson, R. J. Harrison, H. Sekino, B. Sundahl, G. Beylkin, G. I. Fann, S. R. Jensen, and I. Sagert, "On derivatives of smooth functions represented in multiwavelet bases," J. Comput. Phys.: X **4**, 100033 (2019).
[57]F. A. Bischoff, "Regularizing the molecular potential in electronic structure calculations. I. SCF methods," J. Chem. Phys. **141**, 184105 (2014).
[58]M. Schuld, V. Bergholm, C. Gogolin, J. Izaac, and N. Killoran, "Evaluating analytic gradients on quantum hardware," Phys. Rev. A **99**, 032331 (2019).
[59]J. S. Kottmann, A. Anand, and A. Aspuru-Guzik, "A feasible approach for automatically differentiable unitary coupled-cluster on quantum computers," Chem. Sci. **12**, 3497 (2021).
[60]A. Anand, P. Schleich, S. Alperin-Lea, P. W. K. Jensen, S. Sim, M. Díaz-Tinoco, J. S. Kottmann, M. Degroote, A. F. Izmaylov, and A. Aspuru-Guzik, "A quantum computing view on unitary coupled cluster theory," Chem. Soc. Rev. **51**, 1659 (2022).
[61]J. Tilly, G. Jones, H. Chen, L. Wossnig, and E. Grant, "Computation of molecular excited states on IBM quantum computers using a discriminative variational quantum eigensolver," Phys. Rev. A **102**, 062425 (2020).
[62]J. Romero, R. Babbush, J. R. McClean, C. Hempel, P. J. Love, and A. Aspuru-Guzik, "Strategies for quantum computing molecular energies using the unitary coupled cluster ansatz," Quantum Sci. Technol. **4**, 014008 (2018).
[63]Y. S. Yordanov, D. R. M. Arvidsson-Shukur, and C. H. W. Barnes, "Efficient quantum circuits for quantum computational chemistry," Phys. Rev. A **102**, 062612 (2020).
[64]A. Peruzzo, J. McClean, P. Shadbolt, M.-H. Yung, X.-Q. Zhou, P. J. Love, A. Aspuru-Guzik, and J. L. O'Brien, "A variational eigenvalue solver on a photonic quantum processor," Nat. Commun. **5**, 4213 (2014).
[65]J. R. McClean, J. Romero, R. Babbush, and A. Aspuru-Guzik, "The theory of variational hybrid quantum-classical algorithms," New J. Phys. **18**, 023023 (2016).
[66]H. R. Grimsley, D. Claudino, S. E. Economou, E. Barnes, and N. J. Mayhall, "Is the Trotterized UCCSD ansatz chemically well-defined?," J. Chem. Theory Comput. **16**, 1 (2019).
[67]H. R. Grimsley, S. E. Economou, E. Barnes, and N. J. Mayhall, "An adaptive variational algorithm for exact molecular simulations on a quantum computer," Nat. Commun. **10**(1), 3007 (2019).
[68]I. G. Ryabinkin, T.-C. Yen, S. N. Genin, and A. F. Izmaylov, "Qubit coupled cluster method: A systematic approach to quantum chemistry on a quantum computer," J. Chem. Theory Comput. **14**, 6317 (2018).
[69]A. F. Izmaylov, M. Díaz-Tinoco, and R. A. Lang, "On the order problem in construction of unitary operators for the variational quantum eigensolver," Phys. Chem. Chem. Phys. **22**, 12980 (2020).
[70]G.-L. R. Anselmetti, D. Wierichs, C. Gogolin, and R. M. Parrish, "Local, expressive, quantum-number-preserving VQE ansätze for fermionic systems," New J. Phys. **23**, 113010 (2021).
[71]H. G. A. Burton, D. Marti-Dafcik, D. P. Tew, and D. J. Wales, "Exact electronic states with shallow quantum circuits from global optimisation," npj Quantum Inf. **9**, 75 (2023).
[72]H. G. A. Burton, "Accurate and gate-efficient quantum ansätze for electronic states without adaptive optimization," Phys. Rev. Res. **6**, 023300 (2024).
[73]S. E. Ghasempouri, G. W. Dueck, and S. De Baerdemacker, "Modular cluster circuits for the variational quantum eigensolver," J. Phys. Chem. A **127**, 8168 (2023).
[74]K. Gratsea, J. S. Kottmann, P. D. Johnson, and A. A. Kunitsa, "Comparing classical and quantum ground state preparation heuristics," arXiv:2401.05306 (2024).
[75]P. Schleich, J. S. Kottmann, and A. Aspuru-Guzik, "Improving the accuracy of the variational quantum eigensolver for molecular systems by the explicitly-correlated perturbative $[2]_{R12}$-correction," Phys. Chem. Chem. Phys. **24**, 13550 (2022).
[76]P. Schleich, J. Boen, L. Cincio, A. Anand, J. S. Kottmann, S. Tretiak, P. A. Dub, and A. Aspuru-Guzik, "Partitioning quantum chemistry simulations with Clifford circuits," J. Chem. Theory Comput. **19**, 4952 (2023).
[77]M. Weber, A. Anand, A. Cervera-Lierta, J. S. Kottmann, T. H. Kyaw, B. Li, A. Aspuru-Guzik, C. Zhang, and Z. Zhao, "Toward reliability in the NISQ era: Robust interval guarantee for quantum measurements on approximate states," Phys. Rev. Res. **4**, 033217 (2022).
[78]J. S. Kottmann, "Molecular quantum circuit design: A graph-based approach," Quantum **7**, 1073 (2023); arXiv:2207.12421 [physics, physics:quant-ph].
[79]J. S. Kottmann and F. Scala, "Quantum algorithmic approach to multiconfigurational valence bond theory: Insights from interpretable circuit design," J. Chem. Theory Comput. **20**, 3514 (2024).
[80]J. M. Foster and S. F. Boys, "Canonical configurational interaction procedure," Rev. Mod. Phys. **32**, 300 (1960).
[81]R. J. Harrison, "Krylov subspace accelerated inexact Newton method for linear and nonlinear equations," J. Comput. Chem. **25**, 328 (2004).
[82]T. H. Dunning, Jr., "Gaussian basis sets for use in correlated molecular calculations. I. The atoms boron through neon and hydrogen," J. Chem. Phys. **90**, 1007 (1989).
[83]J. Paldus, P. Piecuch, L. Pylypow, and B. Jeziorski, "Application of Hilbert-space coupled-cluster theory to simple $(H_2)_2$ model systems: Planar models," Phys. Rev. A **47**, 2738 (1993).

16 October 2026 14:53:26

© Author(s) 2026